International Forum on Aeroelasticity and Structural Dynamics
IFASD 2017
25-28 June 2017, Como - Italy

PARAMETRIC FLUTTER MARGINS OF A TWIN TAIL CONFIGURATION IN WING-GENERATED BUFFET

Moti Karpel[1] ,Federico Roizner[1], Robert Carrese[2], and Pier Marzocca[2]

[1] Faculty of Aerospace Engineering
Technion, Haifa, 32000, Israel
karpel@technion.ac.il

[2] School of Engineering, RMIT University
Bundoora VIC, 3083, Australia
robert.carrese@rmit.edu.au

Keywords: Flutter, Aeroelasticity, CFD, FSI

Abstract: The recently developed parametric flutter margin (PFM) method is combined with the increase-order modeling (IOM) approach to facilitate stability analysis of nonlinear aeroservoelastic systems with computational fluid dynamics (CFD)-based aerodynamics. The IOM-based Dynresp code is utilized to exchange data with the Fluent CFD code at various fidelity and coupling levels and some features are applied to flutter analysis of a twin-tail configuration under wing-generated buffet loads. Being based on dynamic response to external excitation while the aeroelastic equation of motion is augmented by a stabilizing parameter, the PFM method may significantly improve flutter analyses with nonlinear CFD-based aerodynamic models. However, aeroelastic CFD simulations might induce buffet loads that excite the structure adding noise to the PFM calculations. The main purpose of the work described in this paper was to investigate the effects of the buffet-induced noise on the accuracy of CFD-based PFM predictions. The PFM method is presented in this context and applied to a numerical model of a wind-tunnel of the F/A-18 aircraft. The Dynresp-Fluent assembly is applied to dynamic response cases with and without buffet loads and flutter results are compared with common linear analyses.

1 INTRODUCTION

The increasing complexity of the aerodynamic, structural, control and mechanical components that compose modern aero-servo-elastic (ASE) systems may require high-fidelity simulation models that include important nonlinear effects. The most challenging models are those based on computational fluid dynamics (CFD). While computational fluid-structure-interaction (FSI) techniques are advancing rapidly, they cannot be used as practical design and certification tools in industrial environment due to their prohibiting model preparation and computation time. Hence, common industrial ASE loads and stability analysis tools are mostly linear and applied with conservative margins or safety that might yield reduced performance or late identification of difficulties that require design changes. Numerous reduced order modeling (ROM) techniques that use high-fidelity codes to generate efficient aeroelastic models have been developed in recent years to alleviate the computational burden, but these are often hard to be robustly integrated in common industrial procedures. Another approach that seems to be more successful in industrial environments is the increased-order modeling (IOM) approach [1-3] that starts with linear solutions and then adds nonlinear effects as necessary.

The IOM-based Dynresp framework code solves a linear problem in the frequency domain (FD), adds nonlinear effects and event scenarios in the time domain (TD) and returns to FD in the final step, as detailed in the next section. It was originally developed to facilitate efficient addition of selected nonlinear effects to industrial dynamic loads codes. It has been used in the last 5 years as the main dynamic loads code at Airbus Defence and Space [4], mainly in the A400M project and was recently expanded to perform stability analysis and deal with wake encounter. Being based on the parametric flutter margin (PFM) method [5], the Dynresp stability analysis is based on ASE response to sinusoidal excitation, which facilitates convenient and efficient expansion of the linear flutter and control-margin solutions to nonlinear stability boundaries and limit-cycle oscillation (LCO) characteristics. It can also be very effective for stability predictions in nonlinear regimes, such as in buffeting flow environments, due to strong turbulence interactions often resulting from separating shear layers, unsteady boundary layer interactions, or turbulence vorticity.

The purpose of the work led to this paper was to facilitate various levels of interaction of IOM-based codes with CFD codes. The only requirement from the CFD code is that it can move its aerodynamic grid according to structural surface motion dictated by the progressing structural motion in modal coordinates, and respond with generalized forces applied to these modes in every time step. The Dynresp code is used for this purpose in coupling with the general purpose finite volume code ANSYS Fluent [6] via a sequential pressure-based solver with SIMPLE pressure–velocity coupling, second–order upwind spatial discretization and second–order backward Euler temporal discretization. The SRS model known as Delayed Detached Eddy Simulation (DDES) is used to resolve the turbulent vorticial flow patterns where the SST k-ω turbulence model is used for near wall treatment, similar to the initial study presented in Ref. [7].

This paper discusses the application of the combined Dynresp-Fluent software to PFM flutter analysis of a twin-tail configuration under wing-generated buffet loads. Preliminary dynamic response of a computational model that represents a wind-tunnel experiment was presented in Ref. [8]. Some results are revisited here in the context of response usage in stability analysis, and the PFM method is applied with dynamic responses obtained in various FSI algorithms.

The paper is organized as follows. Section 2 will overview the IOM procedure with emphasis on the various coupling manners with the CFD code. Section 3 will discuss the test cases selected for this study. Section 4 will discuss the PFM procedure and its application in linear flutter analysis with no buffet noise. Section 5 will add the buffet calculated with rigid structure as noise that introduces inaccuracies to the flutter predictions. Section 6 will discuss the extraction of buffet with FSI effects obtained by the tight and loose coupling procedures, and the continuation steps to be performed for fully nonlinear stability analysis with buffet loads.

2 INCREASED-ORDER MODELING IN DYNRESP

The IOM framework [1] used in this work presents systematic methodology and computational tools that exploits the numerical advantages in dealing with linear systems while keeping the complexity of the added nonlinear elements as low as required for obtaining adequate accuracy in aeroelastic analysis. The model, schematically depicted in Fig. 1, is based on a main linear block that is stable when disconnected from the nonlinear elements, and a nonlinear block that expresses all the nonlinearities as feedback loops. The response calculations are performed in 3 stages: (a) response of the linear block with the nonlinear

block disconnected; (b) addition of nonlinear effects using nonlinear elements and convolution integrals; and (c) complementary response of the linear block to inputs from the nonlinear block to generate the final output. The CFD box on the left side of Fig. 1 is connected to the diagramed blocks in the three ways discussed in Section V.

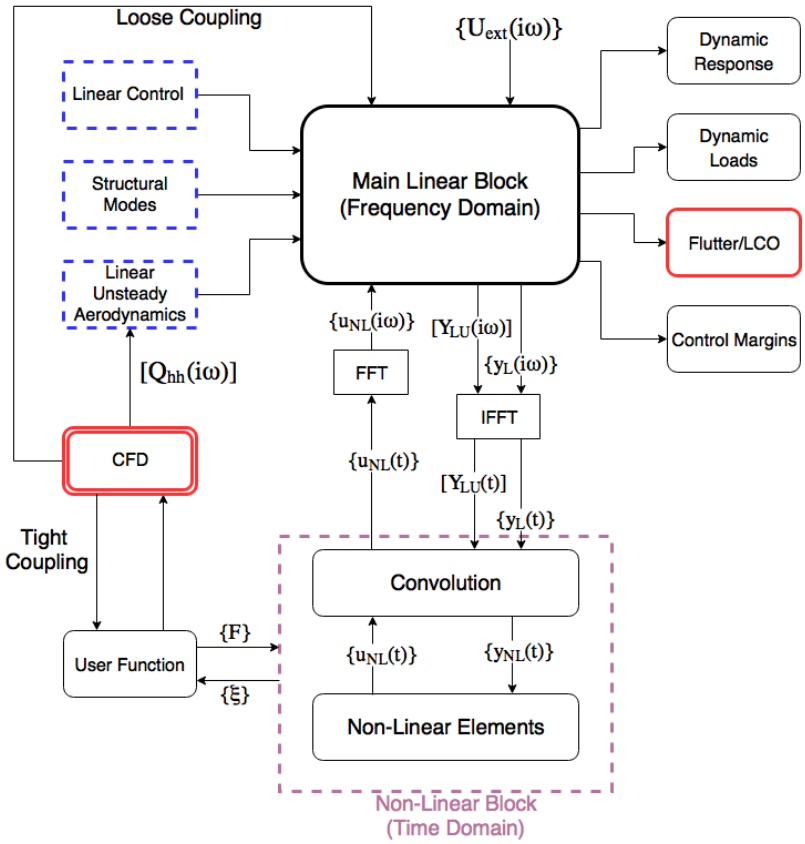

Figure 1: IOM block diagram with CFD-based data.

The first stage is performed in the linear block in Fig. 1, based on FD response to external excitation

$$\{x_L(i\omega)\} = [A(i\omega)]^{-1}[B_{ext}(i\omega)]\{u_{ext}(i\omega)\} \tag{1}$$

where $\{x_L(i\omega)\}$ is the FD vector of modal displacements $\{\xi\}$, actuator outputs $\{\delta\}$ and control states $\{x_c\}$, $\{u_{ext}(i\omega)\}$ is the vector of external inputs, $[A(i\omega)]$ is the closed-loop linear dynamic matrix, and $[B_{ext}(i\omega)]$ is the input distribution matrix. $\{u_{ext}(i\omega)\}$ is obtained via Fast Fourier Transform (FFT) of the input signal $\{u_{ext}(t)\}$. The $\{y_L(i\omega)\}$ outputs of the linear block in Fig. 1, which are inputs to the nonlinear block, can be generally expressed as

$$\{y_L(i\omega)\} = [C(i\omega)]\{x_L(i\omega)\} + [D(i\omega)]\{u_{ext}(i\omega)\} \tag{2}$$

where the coefficient matrices are related to modal displacements and direct-force effects (in the case of acceleration outputs). Other FD response functions are calculated in the linear block in preparation for the subsequent interaction with the nonlinear block. Frequency response of the state vectors $\{x_L(i\omega)\}$ to unit inputs $\{u_{NL}(i\omega)\}$ from the nonlinear block are arranged in the $[x_{LU}(i\omega)]$ matrix and calculated by

$$\left[x_{LU}(i\omega)\right]=\left[A(i\omega)\right]^{-1}\left[B_{NL}(i\omega)\right] \tag{3}$$

from which frequency-response functions $[y_{LU}(i\omega)]$ of the linear output vector to unit inputs from the nonlinear block are calculated by

$$\left[y_{LU}(i\omega)\right]=\left[C_{LU}(i\omega)\right]\left[x_{LU}(i\omega)\right]+\left[D_{LU}(i\omega)\right] \tag{4}$$

To complete the first stage and generate the interim outputs of the linear block in Fig. 1, the linear FD responses of Eqs. (2) and (4) are transformed to TD by

$$\left\{y_L(t)\right\}=IFFT\left\{y_L(i\omega)\right\} \tag{5}$$

and

$$\left[y_{LU}(t)\right]=IFFT\left[y_{LU}(i\omega)\right] \tag{6}$$

where the zero-frequency singularity of the ASE matrix, $[A(0)]$, associated with rigid-body motion, is resolved by transforming the variables to flight mechanic ones. The second stage is performed in the nonlinear block of Fig. 1. The time t is set back to zero and a time-marching nonlinear computation of the outputs $\{u_{NL}(t)\}$ of the nonlinear block is performed in consecutives time steps. The outputs $\{y_L(t)\}$ of the linear block are amended in each time step by the convolution integral

$$\left\{y_{NL}(t)\right\}=\left\{y_L(t)\right\}+\int_0^t\left[y_{LU}(t-\tau)\right]\left\{u_{NL}(\tau)\right\}d\tau \tag{7}$$

and serve as inputs to the nonlinear functions (*NLF*) in the following time step

$$\left\{u_{NL}(t)\right\}=NLF\left\{y_{NL}(t)\right\} \tag{8}$$

which may require some sub iterations when $\{u_{NL}(t)\}$ includes direct forces and $\{y_{NL}(t)\}$ includes accelerations. In the cases demonstrated in this paper, all the inputs in $\{u_{NL}(t)\}$ are direct forces but none of the outputs in $\{y_{NL}(t)\}$ are acceleration related, hence no sub iterations are needed.

The computation process returns in the third stage to the linear block of Fig. 1. The second-stage output $\{u_{NL}(t)\}$ of Eq. (8) is converted to FD by FFT and the final response is calculated by

$$\left\{x_{NL}(i\omega)\right\}=\left\{x_L(i\omega)\right\}+\left[A(i\omega)\right]^{-1}\left[B_{NL}(i\omega)\right]\left\{u_{NL}(i\omega)\right\} \tag{9}$$

followed by

$$\left\{x_{NL}(t)\right\}=IFFT\left\{x_{NL}(i\omega)\right\} \tag{10}$$

This final TD state response may be used for calculating any desired output that is a function of $\{x_{NL}(t)\}$.

3 TEST CASES

A. General

Unlike previous PFM studies that demonstrated flutter and LCO cases where the linear unsteady aerodynamic forces are due to structural vibrations only [5] or with low-level noise in wind-tunnel tests [9], the current study attempts to apply the PFM method with large buffet loads that are affected by the structural vibrations. The purpose was to study the method limits and pointing out some challenges involving the inevitably low signal-to-noise ratio. The F/A-18 twin-tail configuration is used as a test case in this study because of the large buffet loads induced at high angles-of-attack (AOA) maneuvers on the tails due to wing-vortex burst. Even though such dynamic loads do not appear at other flight maneuvers, particularly not at high-speed-low-AOA cases where flutter is more likely, the high buffet loads are applied in most cases of this study to reflect worst-case scenarios.

A wind-tunnel test performed to investigate the twin-tail buffet loads, and some numerical CFD solutions used for complementing that research, are described in Ref. [8]. The CFD and aeroelastic models used in [8] are also used here. The vertical tail of the model is flexible, with the rest of the structure assumed to be rigid. Fig. 2 shows the aerodynamic shape used in constructing the CFD model.

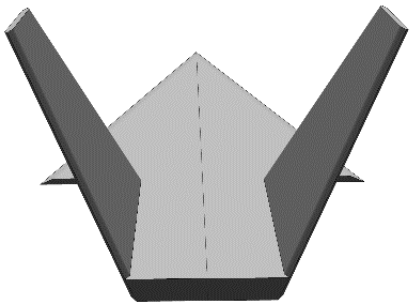

Figure 2: General view of the wind-tunnel configuration.

B. CFD model and flow conditions

The flow conditions were selected such that leading-edge vortices develop and burst, interacting strongly with the vertical tails. Table 1 presents the freestream conditions used in the CFD study.

Parameter	***Value***
Freestream velocity	*40* [m/s]
Freestream air density	*1.225* [kg/m^3]
Dynamic viscosity	*1.8×10^{-5}* [Pa s]
Characteristic length	*0.22* [m]
Reynolds number	*6×10^5*
Angle of attack	*30* [deg]

Table 1: Flow conditions of the full-scale and wind-tunnel models.

The use of the SRS (i.e. DDES) strategy is to ensure the system does not exhibit tonal behavior under breakdown, a result of the ensemble averaging process when solving the

Reynolds-Averaged Navier-Stokes (RANS) equations. This solution strategy would result in a periodic single-harmonic loading, where the characteristic frequency of breakdown is dictated by the change in mean flow conditions, as opposed to the presence of disparate turbulence scales. By contrast, the DDES model results in a broadband excitation of the vertical tail, with a distinct peak referencing the dominant frequency of breakdown.

The flow pathlines of the leading edge vortex as it propagates downstream towards the tail are show in Fig. 3 for the wind-tunnel model. Initially, just downstream of the tip, the flow is characterized by a well defined vortex with high gradients. Just upstream of the tail the vortex can be seen to burst, this is indicated by a sudden increase in the size of the swirling region and low velocity gradients.

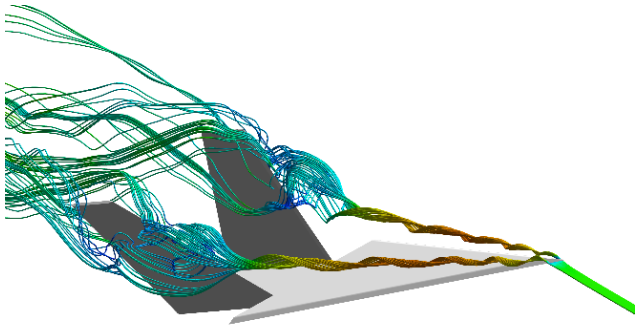

Figure 3: Flow pathlines indicating position of vortex burst forward of vertical-tails.

C. Aeroelastic model

The structural model was based on a clamped flexible tail with the rest of the model kept rigid. Since the excitation is assumed to be symmetric in this study, the two tails move symmetrically. The undamped structural models were generated using the ANSYS Mechanical R18 using shell elements. The model is designed to achieve the first two natural frequencies (i.e. bending and torsion) to coincide with those observed from ground vibration experiments. A total of four modes are selected to describe the dynamics of the vertical tail. The mode shapes are projected from the dynamic (i.e. shell) grid to the aerodynamic grid via MPC184 connections. These connections consist of connecting each dynamic (master) node to local aerodynamic slave nodes to ensure smooth projection of the mode shapes. The first 4 natural frequencies are listed in Table 2. The projected mode shapes for first bending and first torsion are shown in Fig. 4.

Mode	**Frequency [Hz]**
First bending	20.5
First torsion	70.7
Second bending	113.5
Second torsion	176.5

Table 2: Natural frequencies and mode descriptions.

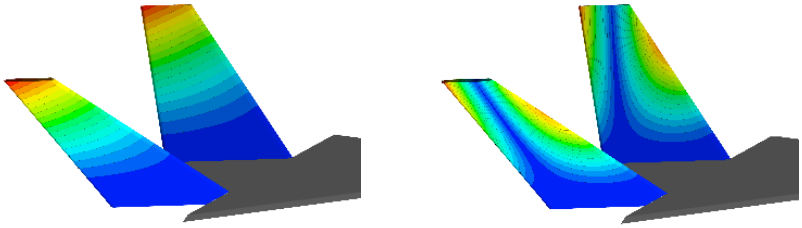

Figure 4: First bending and first torsion modes projected on to the aerodynamic OML.

Two views of the panel model for linear response analysis, generated using ZAERO, are shown in Fig. 7. The generalized aerodynamic force coefficients calculated with this linear model were practically the same to those calculated from the CFD from indicial responses [8]. The red point mark the location of an added mass term introduced for the PFM solution discussed in Section 4.

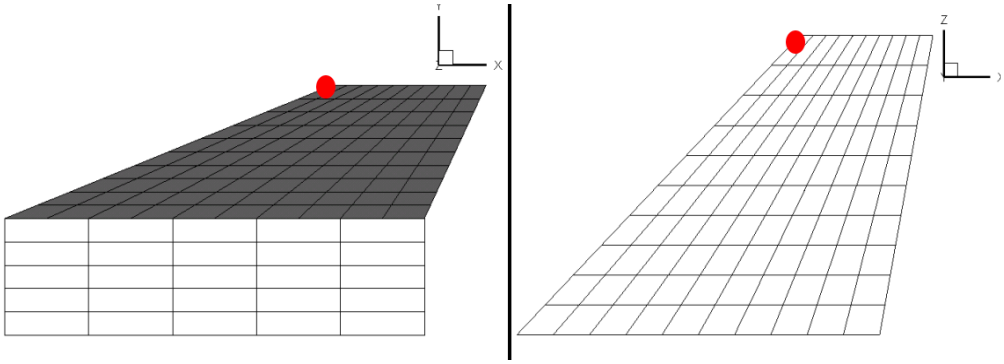

Figure 5: Linear panel model with added mass.

4 LINEAR PARAMETRIC FLUTTER MARGINS WITH NO BUFFET

A detailed development of the PFM method for flutter and LCO analyses is given in Refs. [5, 10]. It is based on adding a stabilizing parameter, P_f, and a control feedback loop that cancels its effects. Response analysis with the loop open is then performed to find the parametric flutter margins at various velocities. Flutter or limit-cycle oscillations (LCO) occur when PFM=0. Being based on dynamic response rather than on the system-matrix singularity characteristics, PFM facilitates a direct coupling process with CFD. The main PFM equation of motion is

$$[A(i\omega)+P_f\{B_f\}[C_f(i\omega)]]\{\xi(i\omega)\} = \{B_f\}u_f(i\omega) \quad (11a)$$

$$y_f(i\omega) = [C_f(i\omega)]\{\xi(i\omega)\} \quad (11b)$$

where the system matrix $[A(i\omega)]$ contains the generalized mass, damping, stiffness and frequency-depended aerodynamic matrices, $\{\xi(i\omega)\}$ is the vector of modal displacements, u_f and y_f are scalars, input and output of the modified system, and $\{B_f\}$ and $[C_f(i\omega)]$ are the respective distribution vectors. The complex ratio $P_f y_f(i\omega)/u_f(i\omega)$ defines the gain and phase associated with the P_f. The velocity at which the there is a cross-over frequency where the phase is $\Phi(\omega_{co}) = 0$ and the phase of $G(\omega_{co}) = 0$dB is the flutter point of the system before being stabilized by the added P_f. The frequency at this point, ω_{co}, is the flutter frequency and the solution $\{\xi(i\omega_{co})\}$ is the flutter mode.

PFM analysis was first applied to the wind-tunnel model of Fig. 2 with a mass term of 10g added in the z direction at the leading edge of the tip section. A unit impulse $u_f(t)$ applied at the same point, also in the z direction, excite the main linear block of Fig. 1. The FFT $u_f(t)$ and that of the co-located acceleration response, $y_f(t)$, was used to produce the flutter gains and phases at various velocities. The effect of the CFD box in Fig. 1 on the PFM calculation were limited at this stage to importing linearized generalized aerodynamic matrices, $[Q_{hh}(i\omega)]$.

The displacement and acceleration response of the added-mass point to unit impulse at t=0.5s at 110m/s are shown in Fig. 6 in TD and FD magnitude. Bode plots of the acceleration response, multiplied by the added mass, are shown in Fig. 7 for various air velocities. The associated flutter gain margins at the cross-over frequencies are plotted in the right side of Fig. 6, indicating the flutter velocity V_f=121.0m/s, where Gain=0dB, and ω_f=51.2Hz. Flutter analysis performed with ZAERO, also with $[Q_{hh}(i\omega)]$ matrices imported from Fluent, indicated practically identical flutter velocity, frequency and mode, as shown in the following sections. The smooth behavior of the gain plot across the nominal flutter velocity indicates that, unlike with the original system, the modified response does not diverge around V_f, which is very important numerically in response calculations using CFD.

5 LINEAR PARAMETRIC FLUTTER MARGINS WITH BUFFET NOISE

We relate in this section to the CFD-buffet loads calculated with rigid structure as "noise" that introduces inaccuracies in the desired response to PFM excitation. The possible effects of the structural response will be discussed in Sec. 6. The linear response to buffet noise is calculated simply by adding the Fourier Transform $\{F_{bR}(i\omega)\}$ of the generalized rigid buffet forces $\{F_{bR}(t)\}$ to the right side of Eq. (11a).

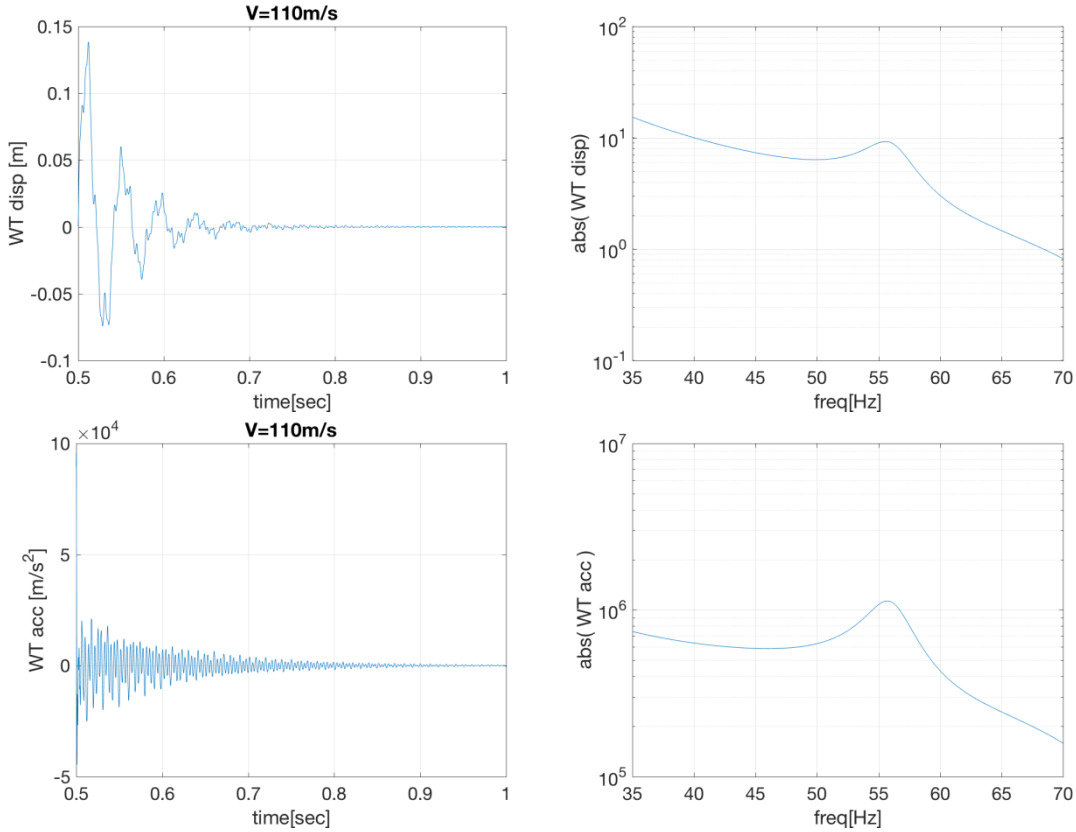

Figure 6: Tip displacement and acceleration at V=110m/s in response to unit impulse at t=0.5s.

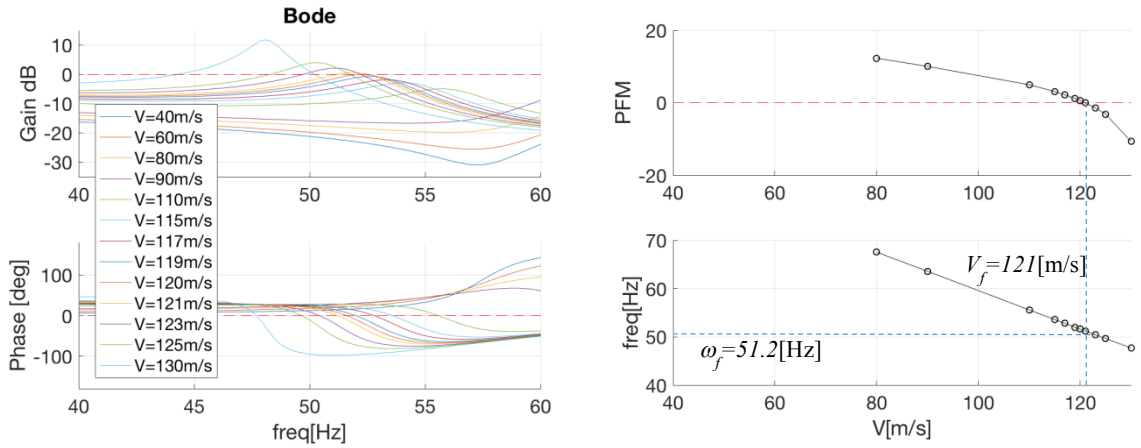

Figure 7: Flutter gain and phase at various velocities and the associated frequency-cross-over and flutter margins.

The TD rigid generalized buffet forces on the first two modes, and the first singular value of their power-spectral-density (PSD) matrix, calculated in Ref. [8], are shown in Fig. 8. It can be observed that there is large excitation between the linear-flutter frequency, 51.2 Hz. and the 1st torsion frequency, 71 Hz. Hence, it is expected that large PFM excitations will be required to overcome the response noise.

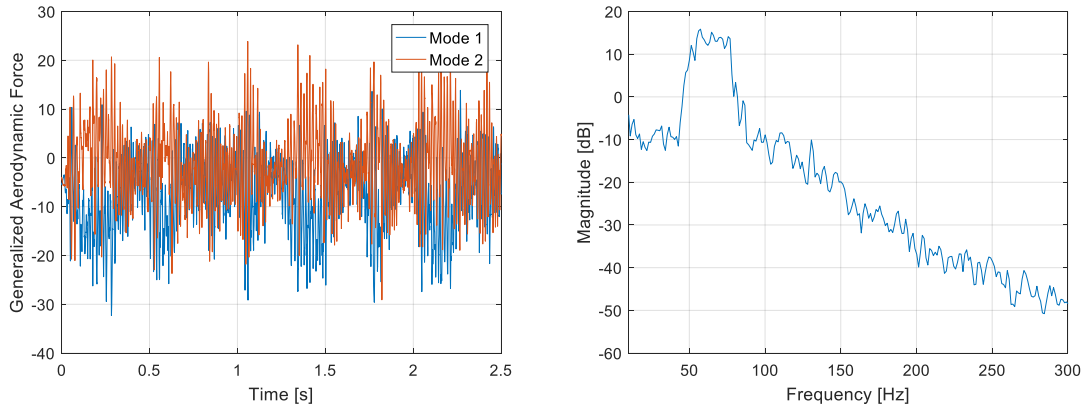

(a) (b)

Figure 8: Generalized aerodynamic forces of the first two modes under rigid constraints: a) time-history; b) first singular value of the power-spectral density matrix.

The acceleration response to unit-impulse PFM excitation was repeated with the buffet noise. The resulting FD acceleration responses shown in Fig. 9 indicate that the PFM excitation force should be increased. To avoid large deformations in subsequent FSI-CFD runs, the impulse-based white-noise excitation was also limited to the 45-55Hz. range. After checking that without noise the PFM results of Fig. 7 are repeated exactly, the calculations were performed with the noise added.

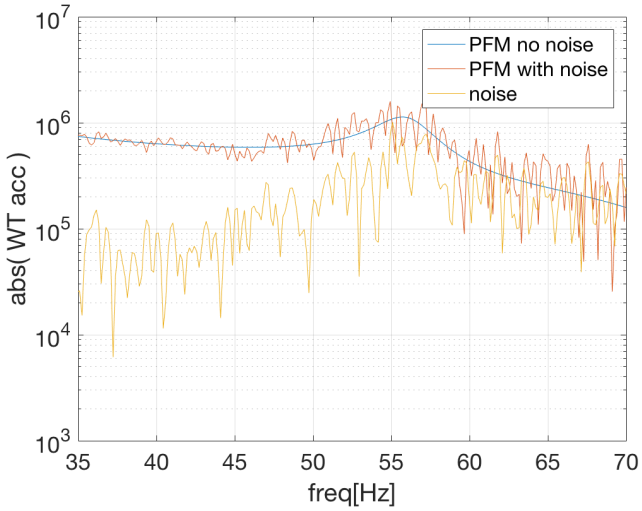

Figure 9: Tip acceleration at V=110m/s in response to unit impulse at t=0.5s and rigid buffet noise.

The resulting Bode plots in the range of 45-55 Hz. are shown in Fig. 10. Even though they are very noisy, they can still be used to extract approximate cross-over frequencies and flutter gains. The resulting parametric flutter margins and the related frequencies vs. velocity are plotted in Fig. 11 in comparison with those of Fig. 7. Even though the plots were based on the plots of Fig. 10 with no smoothing, it can be observed that the resulting PFM and frequency plots are fairly smooth. The marked *PFM*=0dB points with and without noise indicate the respective flutter velocities, which lead to the flutter frequency and modes as discussed above. These flutter characteristics are compared to the ZAERO ones in Table 3. It can be observed that the no-noise Dynresp PFM results are practically identical to those of ZAERO, and that the results under rigid buffet are not very far off considering the level of the resulting buffet vibrations.

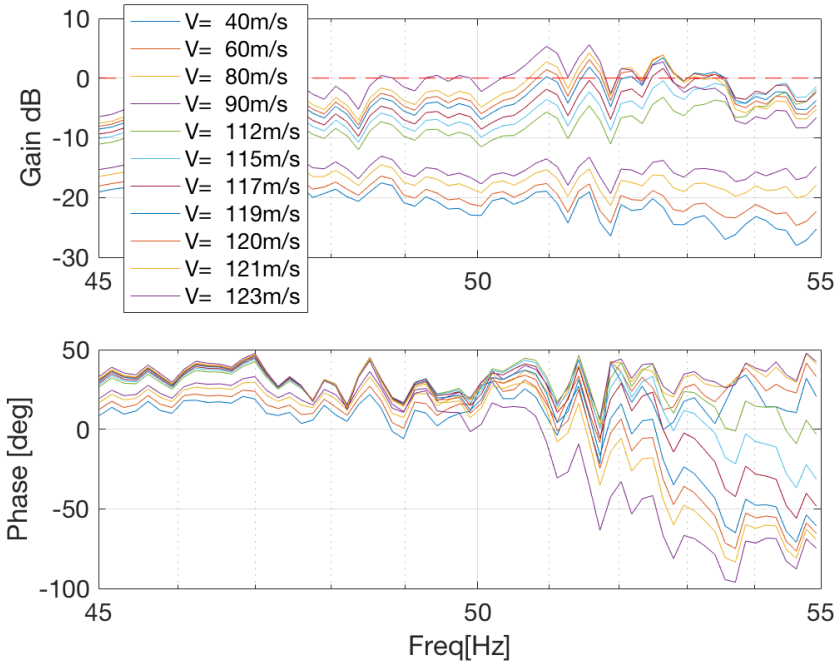

Figure 10: Flutter gain and phase at various velocities with rigid buffet noise.

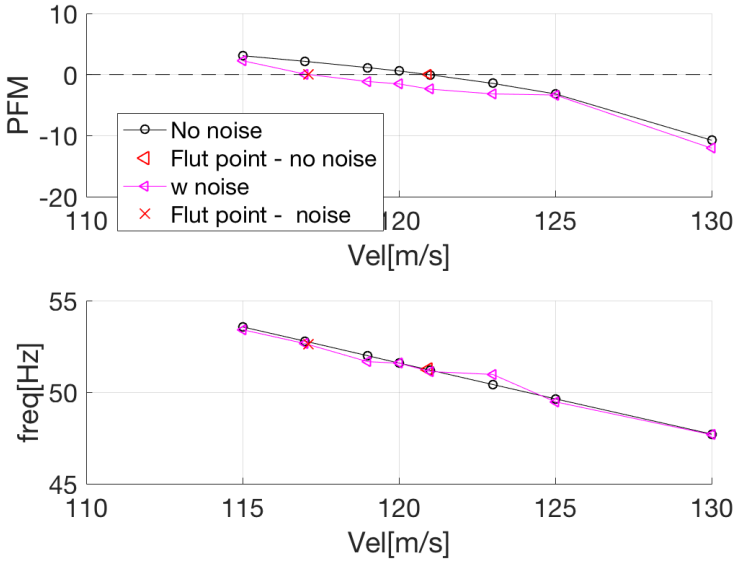

Figure 11: Parametric flutter margins and cross-over frequencies with and without noise.

	ZAERO	PFM	PFM with noise
V_f [m/s]	120.60	120.95	117.10
Diff [%]	--	-0.29	2.90
ω_f[Hz]	51.37	51.22	52.60
Diff [%]	--	0.30	-2.39

	ZAERO		PFM		PFM with noise	
Mode #	Real	Imag	Real	Imag	Real	Imag
1	0.9009	0.3575	0.9137	0.3604	0.8208	0.3252
2	1	0	1	0	1	0
3	0.0394	0.0313	0.0395	0.0312	0.0369	0.0328
4	-0.0064	0.0118	-0.0065	0.0117	-0.0047	0.0104
5	0.0028	-0.0032	0.0029	-0.0032	0.0024	-0.0032
6	0.0012	-0.0017	0.0012	-0.0017	0.0007	-0.0016
7	-0.0026	0.0024	-0.0027	0.0024	-0.0024	0.0024

Table 3: Flutter velocity, frequency and mode calculated using ZAERO and Dynresp-PFM with and without rigid buffet noise.

6 BUFFET WITH FLUID-STRUCTURE INTERACTION

A more accurate investigation of the aeroelastic stability under buffet loads should take into account the nonlinear effects of the structural vibrations on the unsteady aerodynamic loads. The IOM procedure described in Sec. 3 has been expanded for this purpose by interfacing the CFD box in Fig. 1 with the nonlinear-IOM block for a tightly coupled solution, or by extracting excitation data from CFD for a loosely coupled solution. The process that tightly couples Dynresp and Fluent is sketched in Fig. 12. ANSYS Mechanical is used for calculating normal modes and an “RBE3” post processor project the modes on the CFD surface grid. A Python interface transforms modal displacements from Dynresp into surface

displacements in Fluent, and local pressures from ANSYS into generalized forces in Dynresp at every time step.

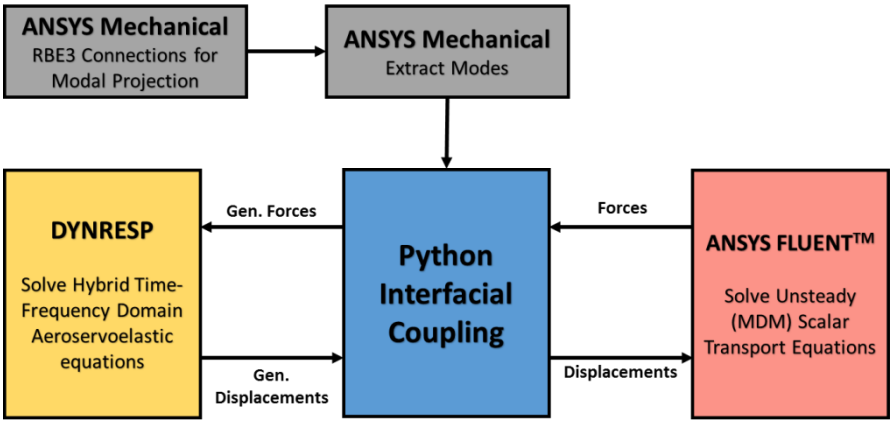

Figure 12: Tight coupling block diagram.

The imported generalized aerodynamic forces from Fluent are introduced to the response analysis in Dynresp as a sequence of correcting impulses and convolution integrals as in Eq. (7). The resulting FD equation of motion in each step is actually

$$(-\omega^2[M_{hh}] + i\omega[C_{hh}] + [K_{hh}] + q[Q_{hh}(ik)])\{\xi_n(i\omega)\} = \{F_{h,n}(i\omega)\} + q[Q_{hh}(ik)]\ \{\xi_{n-1}(i\omega)\} \quad (12)$$

where $[M_{hh}]$, $[C_{hh}]$ and $[K_{hh}]$ are the generalized mass, damping and stiffness matrices. $[Q_{hh}(ik)]$ is the linear unsteady aerodynamic force coefficient interpolated from tabulated matrices at selected reduced frequencies $k_t=\omega_t b/V$. These matrices are can be either extracted from Fluent [8], as indicated in Fig. 1, or imported from external codes.

Since tight-coupling simulations of Fig. 12 have not been available by the time this paper was submitted, we present here the FSI simulations performed in Ref. [8] with the same nominal test case. The difference is that the FSI simulations there were performed in TD using an equivalent Runge-Kutta solution. The resulting generalized displacements and forces, see below, are expected to be practically identical to those of the Dynresp-Fluent process.

The loosely coupled iterative process starts with the rigid buffet forces $\{F_{h,1}\}$, shown in Fig. 8 for the first 2 modes, applied to the linear model as dictated generalized forces for the entire simulation. Eq. (12) is solved in this step with n=1 and $\{\xi_0\}=\{0\}$. The resulting $\{\xi_1(t)\}$ is transferred to the CFD code that is run with pre-dictated deformations to produce $\{F_{h,2}\}$ for the 2nd iterations, and so on. This was performed with the Dynresp-Fluent process in Fig. 12, but with the data transferred every iteration instead of every time step. The results of the first 2 iterations (blue) are compared in Fig. 13 to those of the tight FSI. It can be observed that there is a significant difference between the response in the 1st and 2nd loose-coupling iterations. While the bending displacements reduce, the torsional displacements increase, with both getting closer to the tight FSI results. Reference [8] showed that the increasing torsional vibrations are mainly with frequency close to the 1st-torsion frequency (71 Hz.) due to lock-in phenomena.

The tight FSI process is more efficient that the sequence of loosely-coupled solutions. However the loose coupling process may provide better insight, and can be performed with

CFD and aeroelastic response calculations performed totally separately on different machines.

The responses of this section should be repeated for various velocities with PFM excitation, such as that of Sec. 5, to produce the necessary response data for PFM analysis. Being nonlinear in nature, the results will depend on the excitation level, which may produce nonlinear flutter. These are subjects for future research to be performed with the tightly coupled FSI process of Fig. 12.

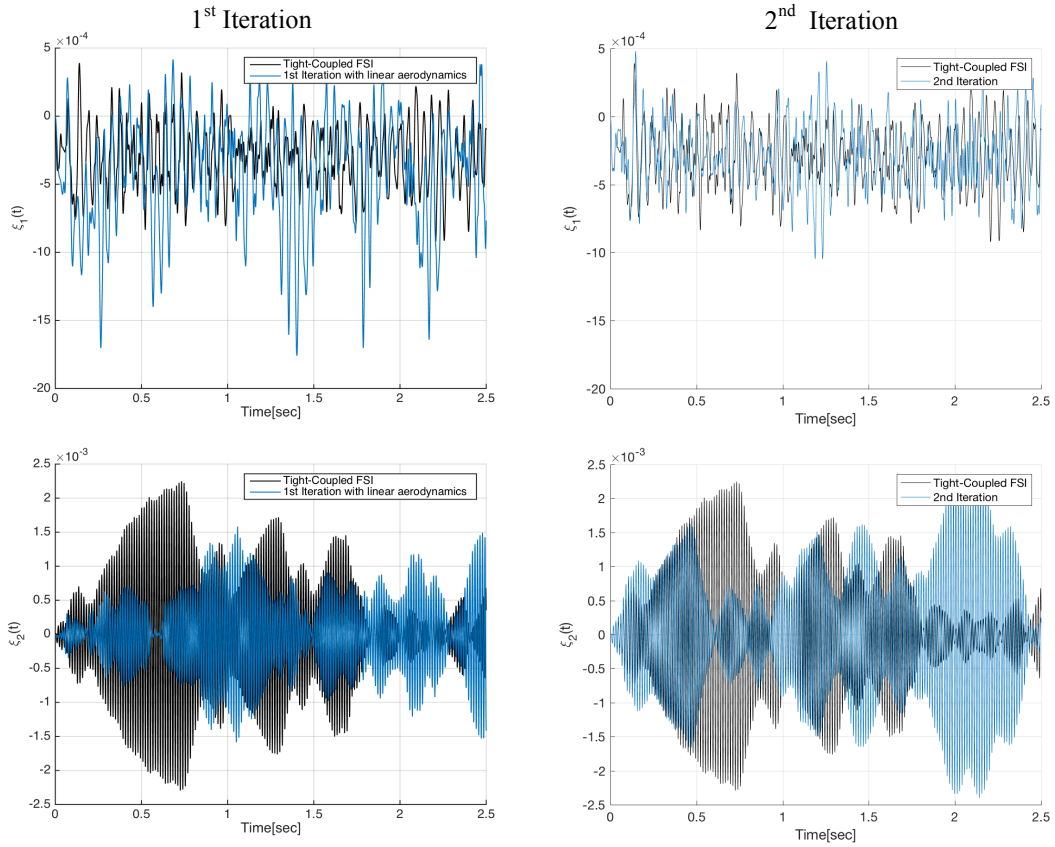

Figure 13: Modal displacements in the loosely coupled process.

REFERENCES

[1] Karpel, M., "Increased-Order Modeling Framework for Nonlinear Aeroservoelastic Analysis," Proceedings of the International Forum on Aeroelasticity and Structural Dynamics, AIAA Paper 2011-73, June 2011.

[2] Karpel, M., and Shousterman, A., "Combined Frequency and Time- Domain Solutions for Aeroservoelastic Response with Nonlinearities," Proceedings of the International Forum on Aeroelasticity and Structural Dynamics, AIAA, Bristol, England, U.K., June 2013.

[3] Karpel, M., Shousterman, A., Maderuelo, C., and Climent, H., "Dynamic Aeroservoelastic Response with Nonlinear Structural Elements," *AIAA Journal*, Vol. 53, No. 11, November 2015.

[4] Reyes, M., Climent, H., Karpel, M., Arévalo, F., and Maderuelo, C., "Increased-Order Aeroservoelastic Modeling In Practice," Proceedings of the International Forum on Aeroelasticity and Structural Dynamics, AIAA, Como, Italy, June 2017.

[5] Roizner, F. and Karpel, M., "Linear and Nonlinear Flutter Analyses Using Dynamic Response Computations," AIAA-2017-1594, presented at the AIAA Structures, Structural Dynamics and Materials Conference, Grapevine, TX, USA, January 2017.

[6] Workbench Users Guide Release 17, Ansys Academic Research, 2016.

[7] Levinski, O., "Aeroelastic Modelling of Vertical Tail Buffet," *16th Australian International Aerospace Congress*, Melbourne, Australia, 2015.

[8] Roizner, F., Karpel, M., Carrese, R., Marzocca, P. and Levinski, O., "Towards a Hybrid Time-Frequency Domain Approach for Time-Variant Buffeting Flows", AIAA-2017-0638, presented at the AIAA Structures, Structural Dynamics and Materials Conference, Grapevine, TX, USA, January 2017.

[9] Sodja, J., Roizner, F., De Breuker, R., And Karpel, M., "Experimental Investigation Of Flutter Boundary With Controlled Vibration Levels," Proceedings of the International Forum on Aeroelasticity and Structural Dynamics, AIAA, Como, Italy, June 2017.

[10] Roizner, F. And Karpel, M., "Aeroservoelastic Stability Analysis Using Response-Based Parametric Flutter Margins," Proceedings of the International Forum on Aeroelasticity and Structural Dynamics, AIAA, Como, Italy, June 2017.

COPYRIGHT STATEMENT